FURTHER STUDIES OF CUP-BURNER FLAME EXTINGUISHMENT

Fumiaki Takahashi
National Center for Space Exploration Research on Fluids and Combustion
NASA Glenn Research Center, Cleveland, OH 44135 USA
Tel: 216-433-3778; Fax: 216-433-8050; Fumiaki.Takahashi@grc.nasa.gov

Gregory T. Linteris
Fire Research Division, National Institute of Standards and Technology
Gaithersburg, MD 20899 USA
Tel: 301-975-2283; Fax: 301-975-4052; linteris@nist.gov

Viswanath R. Katta
Innovative Scientific Solutions, Inc., Dayton, OH, 45440 USA
Tel: 937-255-8781; Fax: 937-656-4110; vrkatta@erinet.com

ABSTRACT

The structure and extinguishment of heptane-air co-flow diffusion flames formed on a cup burner in normal earth gravity have been studied experimentally and computationally. A gaseous fire-extinguishing agent (CO_2) was introduced gradually into a coflowing oxidizer stream until blowoff-type extinguishment occurred. The measured minimum extinguishing concentration of CO_2 was (19.2 ± 0.8) % in volume fraction. A first attempt was made at numerical simulations with full n-heptane chemistry to reveal the detailed flame structure and suppression processes. Overall features of n-heptane flames resembled those of methane flames studied previously: a peak reactivity spot (reaction kernel) in the flame base was responsible for flame attachment and destabilization processes. The initial fuel (heptane) decomposed at moderate temperatures and disappeared on the fuel side before reaching the high-temperature flame zone, and thus CO, H_2, C_2H_2, CH_4, and C_2H_4 became the major intermediates and fuel fragments burning in the flame zone.

Introduction

The cup burner method, specified in national and international standards [1, 2], has been most widely used [3-11] to determine the effectiveness of gaseous fire-extinguishing agents, typically used in a total flooding fire suppression system. The minimum extinguishing concentration (MEC) of agent in a coflowing oxidizer stream indicates the agent's ability to extinguish a fire at the lowest possible concentration. The MEC measured by the cup burner is then used for determining the minimum design concentration of a gaseous agent by adding a safety margin to the MEC value and then meeting third-party approval requirements for a complete fire extinguishing system [11]. Because of its resemblance to fires, great faith has been placed in the cup-burner MEC values, and many safety codes and standards as well as design practices are based on them. However, fundamental understanding of the flame extinguishment processes for this device is very limited. Clearly, the understanding of fire suppression by chemical inhibitors

*Proceedings of the 16th Annual Halon Options Technical Working Conference (HOTWC), Albuquerque, NM, May 16-18, 2006.

as well as inert-gas agents would be greatly improved if their effect in cup-burner flames was investigated from a fundamental perspective.

In previous papers [12-19], flame suppression characteristics of gaseous fire-extinguishing agents (CO_2, N_2, He, Ar, CF_3H, CF_3Br, Br_2, and metallic compounds) were investigated experimentally and computationally for methane cup-burner flames. The authors revealed that the cup-burner flame extinguishment occurred via an unsteady blowoff process (in which the flame base drifted downstream eventually) rather than the global extinction typical of counterflow diffusion flames. A peak reactivity spot (reaction kernel) formed in the flame base was found responsible for a series of flame destabilization processes (detachment, drifting, oscillation, and extinguishment). An addition of any physically acting agent (CO_2, N_2, He, or Ar) to the air cooled the trailing diffusion flame zone to ≈1700 K, thus reducing the heat and radical transfer rates to the reaction kernel and causing its destabilization. Chemical inhibitors (CF_3H, CF_3Br, Br_2, and metallic compounds) effectively reduced the chain radical (H, O, and OH) supplies to the reaction kernel, leading to the destabilization.

The cup-burner MEC data for heptane liquid fuel are most abundant in the literature because it represents difficult-to-extinguish liquid-fuel fires and its physical properties (e.g., the viscosity and vapour pressure) are suitable for handling in the laboratory. Modeling a liquid hydrocarbon flame becomes challenging if both detailed chemical and physical processes are included. Katta and Roquemore [20] have recently incorporated a detailed n-heptane reaction mechanism and organophosphorus chemistry into the UNICORN (Unsteady Ignition and Combustion using ReactioNs) code [21] for the simulation of premixed (Bunsen) flames and gaseous heptane jet diffusion flames. Because the gas-phase reactions play a decisive role in flame extinguishment by gaseous agents, the use of detailed chemistry is essential for understanding the combustion and suppression processes, even if some physical elements such as the heat feed-back from the flame to the liquid fuel and its vaporization are omitted from the modeling for simplicity.

The overall objectives of the present study are to understand the physical and chemical processes of cup-burner flame extinguishment and to provide rigorous testing of numerical models, which include detailed chemistry and radiation sub-models. This paper reports the experimental and computational results of the structure and extinguishment of gaseous heptane flames using CO_2 as the agent.

Experimental Procedures

The cup burner, described previously [7], consists of a cylindrical glass cup (28 mm outer diameter, 45º-chamfered inside burner rim) positioned inside a glass chimney (8.5 cm or 9.5 cm inner diameter, 53.3 cm height). To provide uniform flow, 6 mm glass beads fill the base of the chimney. For the liquid heptane, a dual syringe-pump (Yale Apparatus model YA-12) feed system provided fuel at measured rates so that the fuel was level with the edge of the cup rim. Gas flows were measured by mass flow controllers (Sierra 860*) which were calibrated so that their uncertainty is 2 % of indicated flow.

*Certain commercial equipment, instruments, or materials are identified in this paper to adequately specify the procedure. Such identification does not imply recommendation or endorsement by NIST or NASA, nor does it imply that the materials or equipment are necessarily the best available for the intended use.

The fuel used is liquid n-heptane (n-C_7H_{16}), and the agent is CO_2 (Airgas, 99.5 %). The air is house compressed air (filtered and dried) which is additionally cleaned by passing it through an 0.01 μm filter, a carbon filter, and a desiccant bed to remove small aerosols, organic vapors, and water vapor. To determine the suppression condition, the agent is added (in increments of < 1 % near extinguishment) to co-flowing air (held at a constant flow rate) until extinguishment occurred. The test was repeated at least three times at each of the different coflow velocities.

An uncertainty analysis was performed, consisting of calculation of individual uncertainty components and root mean square summation of components. All uncertainties are reported as *expanded uncertainties*: $X \pm ku_c$, from a combined standard uncertainty (estimated standard deviation) u_c, and a coverage factor $k = 2$. Likewise, when reported, the relative uncertainty is ku / X. The expanded relative uncertainties for the experimentally determined quantities in this study are 4 % for the volume fractions of CO_2.

Computational Methods

Unsteady computations of the cup-burner flames were performed using a numerical code (UNICORN [21]), as described in detail previously [12, 14]. It solves for axial- and radial-momentum equations, continuity, and enthalpy- and species-conservation equations on a staggered-grid system. The body-force term due to the gravitational field is included in the axial-momentum equation for simulating vertical flames. A clustered mesh system is employed to trace the large gradients in flow variables near the flame surface. A detailed chemical-kinetics model developed by NIST [22] (197 species and 2757 elementary-reaction steps) is incorporated into UNICORN for the investigation of n-heptane flames including polycyclic aromatic hydrocarbon (PAH) formation. In addition, a two-equation model for soot formation with transport equations for particle number density and soot mass fraction is incorporated [20].

Thermophysical properties such as enthalpy, viscosity, thermal conductivity, and binary molecular diffusion of all the species are calculated from the polynomial curve fits developed for the temperature range 300 - 5000 K. Mixture viscosity and thermal conductivity are then estimated using the Wilke and Kee expressions, respectively. Molecular diffusion is assumed to be of the binary-diffusion type, and the diffusion velocity of a species is calculated using Fick's law and the effective diffusion coefficient of that species in the mixture. A simple radiative heat-loss model [23] based on optically thin-media assumption and Plank-mean absorption coefficients for CO_2, H_2O, CH_4, and CO, and soot was incorporated into the energy equation.

The finite-difference forms of the momentum equations are obtained using an implicit QUICKEST scheme [24, 25], and those of the species and energy equations are obtained using a hybrid scheme of upwind and central differencing. At every time step, the pressure field is accurately calculated by solving all the pressure Poisson equations simultaneously and using the LU (Lower and Upper diagonal) matrix-decomposition technique. The boundary conditions are treated in the same way as that reported in earlier papers [12-19].

Calculations are made for full-size and 5/8-scale cup burners. The cup outer diameters are 28 mm and 18 mm, respectively, and the chimney inner diameters are 95 mm and 59.2 mm, respectively. Computational physical domains are 200 mm by 47.5 mm and 100 mm by

29.6 mm, respectively. Non-uniform grid systems of 251 × 101 and 231 × 131 yield 0.2 mm by 0.2 mm and 0.1 mm by 0.1 mm minimum grid spacing, respectively, in both the axial (z) and radial (r) directions in the flame zone. The integration times are 100 μs and 50 μs, respectively. The computational domain is bounded by the axis of symmetry and a chimney wall boundary in the radial direction and by the inflow and outflow boundaries in the axial direction. The outflow boundary in z direction is located sufficiently far from the burner exit (≈15 fuel-cup radii) such that propagation of boundary-induced disturbances into the region of interest is minimal. The burner wall (1-mm- or 2-mm-long and 1-mm-thick tube) temperature is set at 600 K. While the mean fuel velocities used for both the full-size and 5/8-scale burners are 0.94 cm/s and 0.1 cm/s, the fuel jet is surrounded by a constant oxidizer flow with a velocity of 10.7 cm/s.

Results and Discussion

Experimental Observations

Figure 1a shows a video frame image of a heptane-air coflow diffusion flame in a full-size cup-burner apparatus. The following general features of the flame were similar to those for gaseous methane flames observed previously [13, 17], except that the heptane flames were much sootier and longer. The blue flame base anchored at the burner rim with an inward inclination as a result of an overall stream-tube shrinkage due to accelerating buoyancy-induced flow as well as considerably low fuel velocity compared to that of the coflowing air. The color of the flame zone turned bright yellow downstream due to considerable soot formation, thus saturating the video image sensor output. The flame was flickering due to instabilities in the buoyancy-induced flow near the flame zone. As a result, the moving flame downstream was captured in

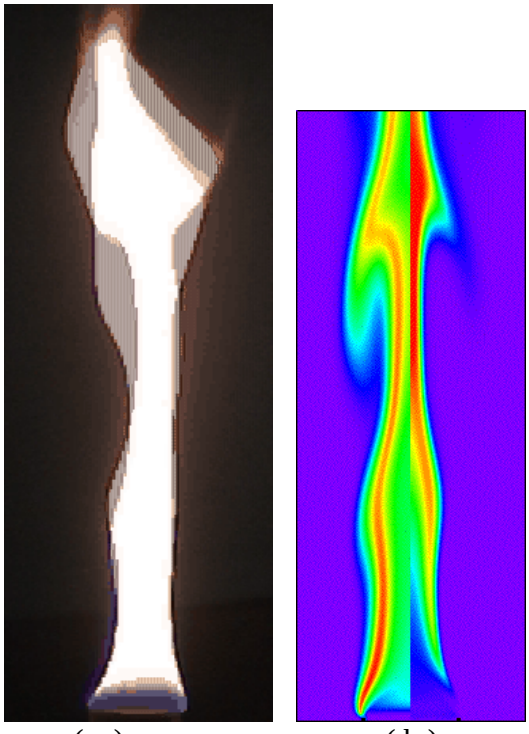

(a) (b)

Fig. 1 (a) A video image and (b) calculated temperature (left) and soot mass fraction (right) contours of a heptane flame on a full-size cup burner.

split images of two fields (60 Hz) consisting the video frame image (30 Hz). As CO_2 was added into coflowing air, the entire flame zone turned blue, and the flame base detached from the burner rim in search of a new stabilization point downstream (in the inward and upward direction). As the CO_2 concentration approached to the extinguishment limit, the flame base oscillated over several millimeters along the streamline direction. As the flame base reached a certain farther location, it was unable to return to the burner rim and thus blew off.

The measured MEC value of CO_2, in volume fraction ($X_{a,exp}$), was (19.2 ± 0.8) %. The value was somewhat low compared to other values in the literature (typically, 0.20 to 0.23) [8-11], possibly due to the relatively low air volumetric flow rate of 25 L/min, in these tests, although MECs are known to exhibit a "plateau region" [1, 5, 6], i.e., insensitivity to the mean oxidizer velocity (U_{ox}), once a minimum flow is achieved. The fuel velocity, fuel-cup diameter, and chimney diameter are also known to have a small or negligible impact on the agent concentration at suppression [5]. The limiting oxygen index, in volume fraction (X_{O2}), calculated from the extinguishing agent volume fraction (X_a) as $X_{O2} = X_{O2,initial}\ (1 - X_a)$, where $X_{O2,initial}$ is the initial oxygen volume fraction in the neat oxidizer (0.2095 for air), was (16.9 ± 0.2) %.

Unlike the previously studied [12-19] gaseous-fuel (methane) flames with a constant fuel flow rate (i.e., velocity), the vaporized liquid fuel (heptane) flow rate decreases with agent addition due to reduced heat feed-back. Figure 2 shows the measured liquid heptane consumption rate in a cup burner as a function of the CO_2 volume fraction in the oxidizer stream. A unit liquid heptane consumption rate (1 mL/min) converts to a gaseous flow rate of ≈0.52 L/min at 294 K. The results in Fig. 1 were influenced by the sooting tendencies of heptane cup-burner flames. Heat transfer to the fuel pool surface was enhanced by soot in the gas phase as well as by soot on the hot chimney walls. At higher volume fraction of added CO_2, soot formation was visually observed to be suppressed.

Computational Results

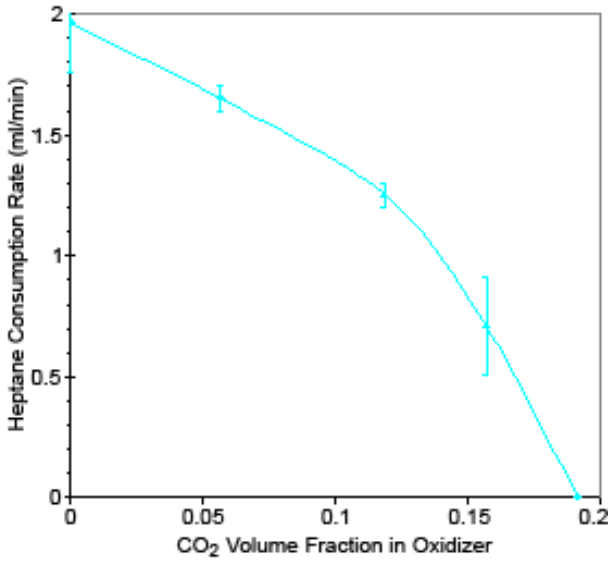

Fig. 2 Measured liquid heptane consumption rate in a full-size cup-burner flame as a function of the CO_2 volume fraction in the oxidizer stream.

Unsteady numerical simulations with full chemistry were conducted for heptane flames on the full-size and 5/8-scale cup burners. Figure 1b shows contours of the calculated temperature (left) and soot mass fraction (right) in a full-size heptane flame at the mean fuel velocity of U_f = 0.94 cm/s (which corresponded to 1.8 mL/min liquid-fuel consumption rate) and an oxidizer velocity of U_{ox} = 10.7 cm/s. The temperature contours (Fig. 1b, left) indicated the evolution and development of large-scale vortices due to buoyancy-induced flow instability, and their wavy structure resembled the video images (Fig. 1a). The soot mass fraction contours (Fig. 1b, right) revealed the general trend that the incipient soot formation started in the high-temperature fuel-pyrolysis zone on the fuel-side of the peak temperature at ≈6 mm above the burner and that the soot mass fraction increased downstream due to a cumulative effect. The results are qualitatively consistent with the experimental observation that the flame zone turned from blue to yellow and increased its intensity downstream. The good qualitative agreement between the observed and predicted dynamic flame behaviors and sooting tendency implied that the complex flow-flame interactions were treated accurately in the numerical model.

The calculated inner structure of the flame attachment region provides more detailed physical and chemical insights into the extinguishment processes. It is advantageous to use the 5/8-scale cup burner with the fine grid system to increase the spatial resolution under the limited computational resources. For the 5/8-scale heptane-fueled cup burner (U_f = 0.1 cm/s and U_{ox} = 10.7 cm/s), Figure 3a shows the calculated structure for pure air, while Figure 3b shows that for air with CO_2 at X_a = 0.07. The variables include, on the right half: velocity vectors (**v**), isotherms (T), total heat-release rate ($\dot{q}$), and the local equivalence ratio (ϕ_{local}); on the left half: the total molar flux vectors of atomic hydrogen ($\mathbf{M}_H$), oxygen mole fraction (X_{O2}), oxygen consumption rate ($-\hat{\omega}_{\mathbf{O2}}$), and mixture fraction (ξ), including stoichiometry (ξ_{st} = 0.062 [X_a = 0] and 0.056 [X_a = 0.07]). The local equivalence ratio is defined [26] by considering a stoichiometric expression for intermediate species in the mixture to be converted to CO_2 and H_2O and is identical to the conventional equivalence ratio in the unburned fuel-air mixture. The mixture fraction was determined by the element mass fractions of carbon, hydrogen, and oxygen as defined by Bilger [27].

The following common features for the burner-rim-attached flame in air (Fig. 3a) and the detaching flame in air with CO_2 (Fig. 3b) are similar to those for methane [17, 18]. The velocity vectors show the longitudinal acceleration in the hot zone due to buoyancy. As a result of the continuity of the fluid, surrounding air was entrained into the lower part of the flame. The entrainment flow inclined inwardly because of the overall stream-tube shrinkage due to the minimal fuel flow compared to the oxidizer flow and the flow acceleration downstream. Both heat-release rate and oxygen-consumption rate contours showed a peak reactivity spot (i.e., the reaction kernel [28]) at the flame base, where the oxygen-rich entrainment flow crossed the flame sheet, thus enhancing convective (and diffusive) contributions to the oxygen flux. On the other hand, chain radical species, particularly the H atom, diffuse back against the oxygen-rich incoming flow at the flame base (edge). As a result, chain-branching ($H + O_2 \rightarrow OH + O$) and subsequent exothermic reactions are enhanced particularly at the flame base, thus forming the reaction kernel.

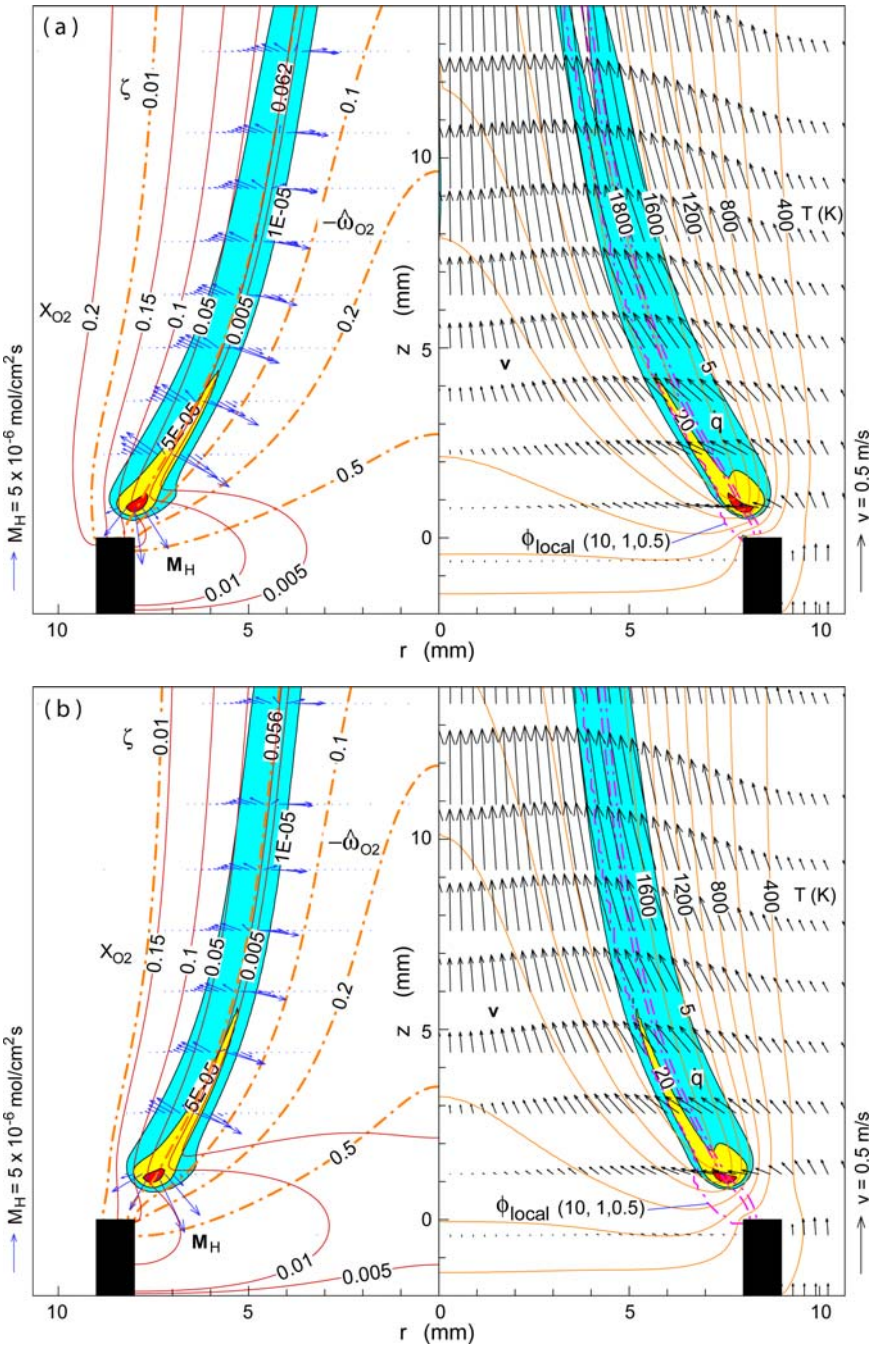

Fig. 3 Calculated structure of heptane flames on a 5/8-scale cup burner. U_f = 0.1 cm/s, U_{ox} = 10.7 cm/s. (a) In air; (b) in air with CO_2, X_a = 0.07. ($\dot{q}$ contours: 5, 20, and 80 J/cm^{3}s; $-\hat{\omega}_{O2}$ contours: 1×10^{-5}, 5×10^{-5}, and 2×10^{-4} mol/cm^{3}s.)

The heat-release rate, oxygen consumption rate, velocity, temperature, oxygen mole fraction, local equivalence ratio, and mixture fraction at the reaction kernel in the flame in air (Fig. 3a) were: $\dot{q}_k$ = 136 J/cm^{3}s, $-\hat{\omega}_{O2,k}$= 0.00035 mol/cm^{3}s, $|\mathbf{v}_k|$ = 0.190 m/s T_k = 1445 K, $X_{O2,k}$ = 0.040, $\phi_{local,k}$ = 0.64, and ξ_k = 0.039, respectively, and with CO_2 (Fig. 3b): $\dot{q}_k$ = 124 J/cm^{3}s, $-\hat{\omega}_{O2,k}$= 0.00032 mol/cm^{3}s, $|\mathbf{v}_k|$ = 0.193 m/s T_k = 1471 K, $X_{O2,k}$ = 0.033, $\phi_{local,k}$ = 0.82, and ξ_k = 0.054.

The reactivity ($\dot{q}$ and $-\hat{\omega}_{O2}$) showed a sharp peak (the reaction kernel) and decreased dramatically in the trailing diffusion flame, whereas the velocity increased downstream by a cumulative effect of the buoyancy-induced flow. Thus, a downstream portion of the flame zone with lower reactivity was supported in series by an upstream portion, with the reaction kernel as the initiating region, as described in detail previously [28]. Without agent, the maximum flame temperature in the trailing diffusion flame (T_{max}) was 1823 K at z = 6.8 mm, which was 451 K lower than the calculated adiabatic flame temperature (T_f) of 2274 K [29] for stoichiometric conditions and X_{O2} = 0.21. The lower peak temperature is due to heat losses, leakage of oxygen (and intermediates) through the flame, and other effects. With 7 % added CO_2, while T_{max} decreased to 1758 K at z = 9.5 mm, which was 385 K lower than T_f. Note that the flames with added CO_2 are cooler and less sooting than the flames without, thus radiating less heat.

Figure 4 shows the variations of the calculated temperature, total heat-release rate, and chain radical mole fractions across the reaction kernel ($z = z_k$ = 0.8 mm, fine curves) and an arbitrarily chosen height in the trailing diffusion flame (z = [z_k + 10] mm = 10.8 mm, thick curves) in a heptane flame on a 5/8th-scale cup burner in air. At the height across the reaction kernel, the maximum temperature was 315 K lower than that in the trailing flame, the radical mole fractions are a factor of >2 smaller, but the maximum heat-release rate was an order of magnitude larger at the reaction kernel for the reason described above.

Figure 5 shows the calculated species mole fractions (X_i) across the trailing diffusion flame (Fig. 5a, z = 10.8 mm) and the reaction kernel (Fig. 5b, z = 0.8 mm) (up to 19 species are shown for clarity). Basic features in the flame structure are similar to methane flames [13, 17] but more complex as a result of a greater variety of fuel fragments, decomposed from the initial fuel on the fuel side. At the reaction kernel height (Fig. 5b), heptane disappeared before reaching the flame

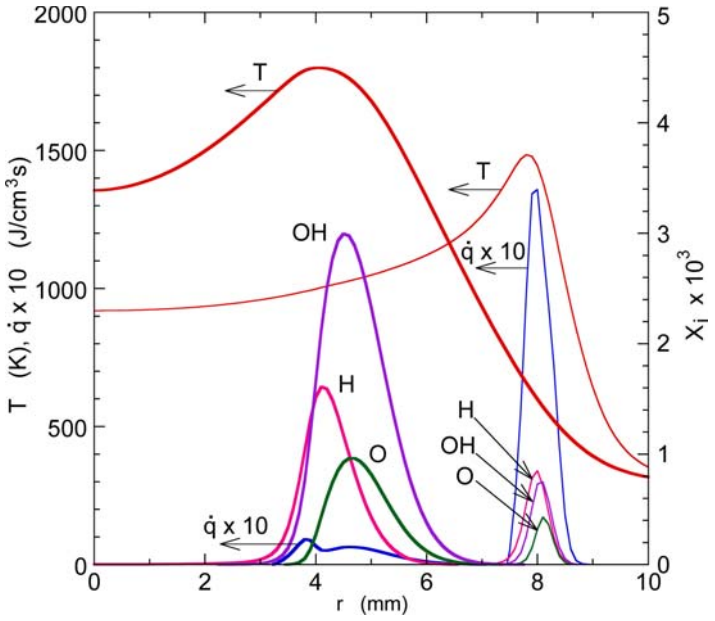

Fig. 4 Calculated temperature, heat-release rate, and radical mole fractions across the reaction kernel (z = 0.8 mm, thin curves) and the trailing diffusion flame (z = 10.8 mm, thick curves) in a heptane flame in air on a 5/8th-scale cup burner.

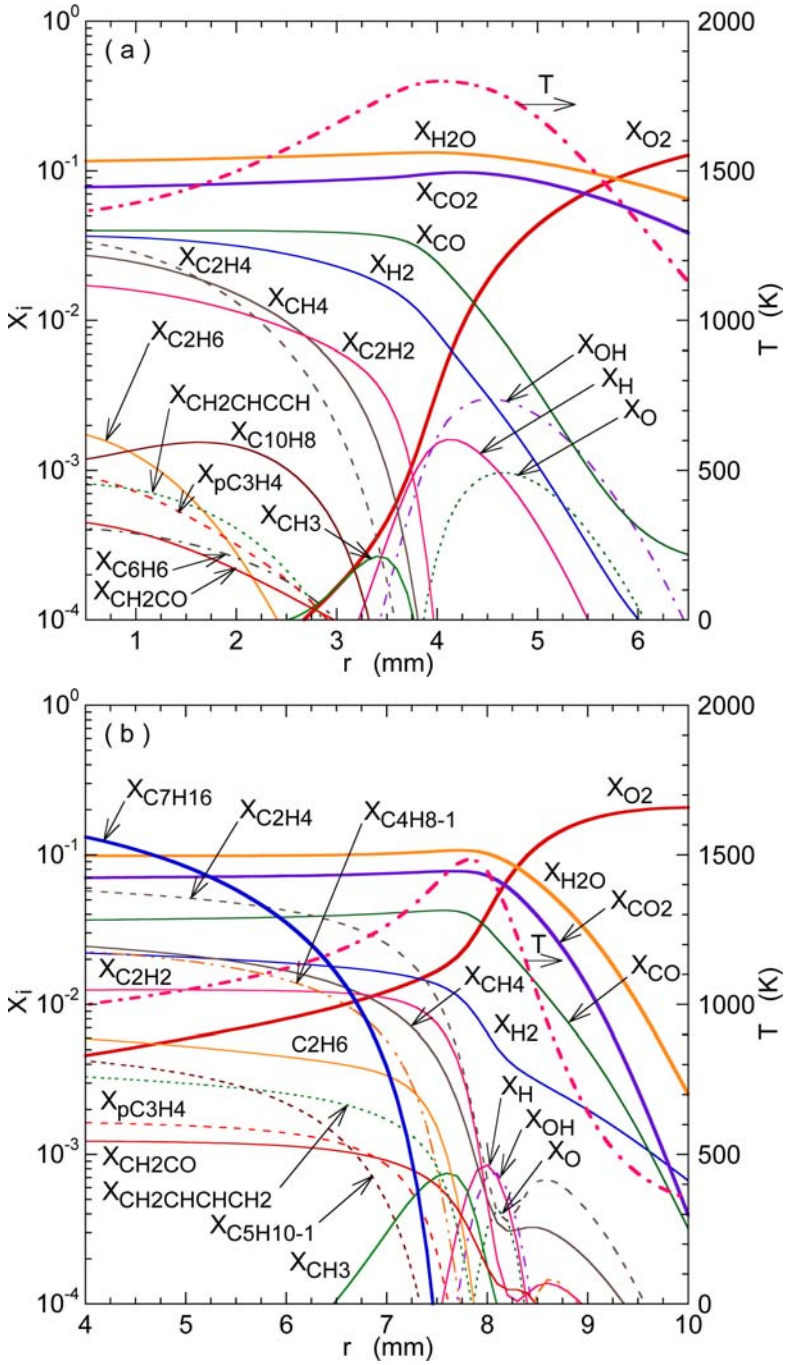

Fig. 5 (a) Calculated mole fractions across the trailing diffusion flame (z = 10.8 mm) and (b) the reaction kernel (z = 0.8 mm) in a heptane flame in air on a 5/8th-scale cup burner.

zone, and the major fragments burning in the flame zone are C_2H_4, C_2H_2, and CH_4 as well as major intermediates (CO and H_2). Similar trends were observed also for propane jet diffusion flames studied previously [30]. C_4-hydrocarbons (1-C_4H_8 and $CH_2CHCHCH_2$), C_2H_6, and CH_2CO are also present in the reaction kernel. A distinct feature at reaction kernel was that the oxygen penetrated into the fuel side through the quenched space, thus resulting in high oxygen concentration around the reaction kernel; also, the fuel fragments (C_2H_4, and CH_4) escaped

through the quenched space onto the air side, thus making small humps in the mole fraction curves.

In the trailing diffusion flame at z = 10.8 mm (Fig. 5a), heptane is not present even on the axis, where the temperature reached 1356 K. Because of the low fuel velocity (long residence time), heptane decomposed at moderate temperatures and disappeared in the central region. The fuel species burning in the trailing diffusion flame zone were CO, H_2, C_2H_2, CH_4, and C_2H_4 in a descending order in their mole fractions. Therefore, the structure of the trailing diffusion flame of any higher-order aliphatic hydrocarbons must be similar, and thus, the effect of an agent, introduced into the oxidizer, on the trailing flame must be similar as well. On the other hand, at the reaction kernel, which controls the destabilization processes, the chemical kinetic structure and the agent effects (particularly, for chemically active agents) must be more dependent on the fuel type.

As the CO_2 volume fraction in the oxidizer was increased to $X_a \approx 0.13$, the detached flame base started to oscillate along the streamline direction. Figure 6 shows a series of the calculated temperature (left) and soot mass fraction (right) contours during an oscillation cycle. The origin of the elapse time (t = 0) was chosen arbitrarily when the flame base was attached to the burner rim. As the flame base detached from the rim and drifted inward (Fig. 6a and 6b), the flame length shortened: the flame-base height increased and the flame-tip height (the maximum temperature on the axis) decreased, and the soot nearly disappeared as the fuel surrounded by the flame zone was being consumed. At the same time, the fuel-air mixing in the widened, low-speed space between the flame base and the burner rim progressed, and the flame base propagated back toward the rim (Fig. 6c and 6d). The oscillation frequency of the base was ≈3 Hz, which was half that for methane flames (6 Hz) [13, 31]. In methane flames, the flame-base oscillation was strongly coupled with the buoyancy-induced vortex evolution at 12 Hz. In the heptane flames, the vortex evolution occurred only in downstream portions of the flame, probably because of the lower fuel velocity and the smaller 5/8th-scale burner. The computations at higher CO_2 volume fractions are currently in progress to determine the extinguishing limit.

Conclusions

The measured minimum extinguishing concentration of CO_2 in heptane flames by using a full-size cup burner was (19.2 ± 0.8) %. The numerical simulations with full n-heptane chemistry have revealed the detailed structure of gaseous heptane cup-burner flames. The initial fuel decomposed at moderate temperatures on the fuel-side of the flame and disappeared before reaching the flame zone. Major fuel species burning in the flame zone were CO, H_2, C_2H_2, CH_4, and C_2H_4. As the CO_2 volume fraction in the coflowing oxidizer was increased, the flame base detached, drifted downstream, and oscillated at ≈3 Hz. Weak buoyancy-driven vortex evolution in the heptane flames appeared to reduce the oscillation frequency, compared with that (6 Hz) for the methane flames studied previously. Better understanding of the chemical-kinetic structure and unsteady physical processes in cup-burner flames should prove useful for extrapolating the laboratory-scale flame phenomena to the fire suppressant needs for full-scale fires.

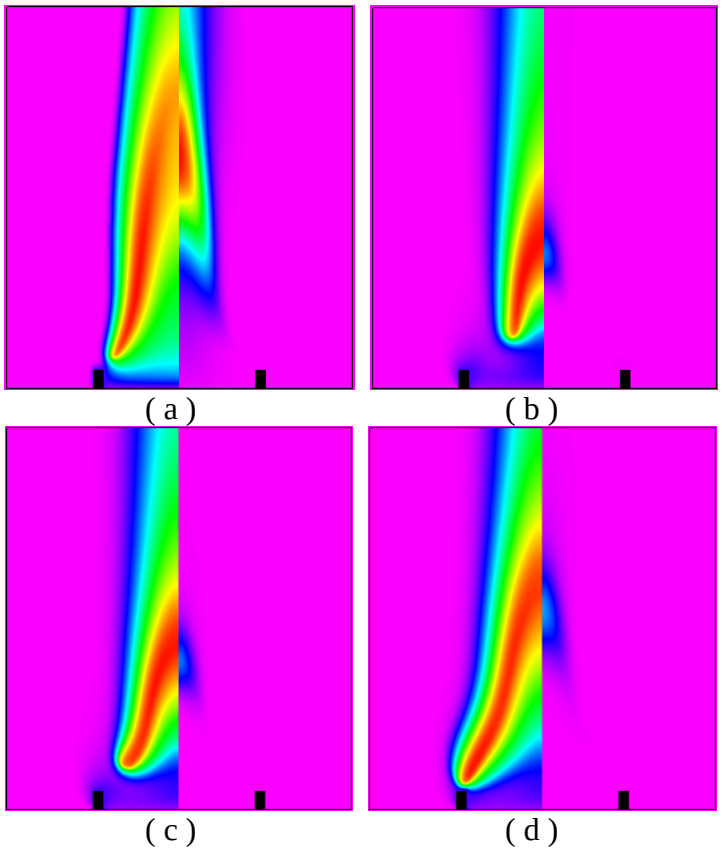

Fig. 6 Calculated temperature (left) and soot mass fraction (right) contours of an oscillating heptane flame in air with CO_2 (X_a = 0.13) on a 5/8th-scale cup burner. Elapse time: t = (a) 0 s, (b) 0.25 s, (c) 0.288 s, (d) 0.313 s.

Acknowledgment

This work was supported by the Office of Biological and Physical Research, National Aeronautics and Space Administration, Washington, DC.

References

1. Anon., *Standard on Clean Agent Fire Extinguishing Systems*, National Fire Protection Association, 2004 Edition, NFPA 2001, Quincy, MA, 2004.
2. Anon., "Gaseous Fire-Extinguishing Systems—Physical Properties and System Design," 2nd Edition, International Organization for Standardization, ISO 14520-Part I, 2006.
3. S. N. Bajpai, *J. Fire and Flammability* 5 (1974) 255.
4. R. Hirst, K. Booth, *Fire Technology* 13 (1977) 4.
5. R. S. Sheinson, J. E. Pener-Hahn, D. Indritz, *Fire Safety Journal* 15 (1989) 437-450.
6. A. Hamins, G. Gmurczyk, W. Grosshandler, R. G. Rehwoldt, I. Vazquez, T. Cleary, C. Presser, K. Seshadri, in: W. L. Grosshandler, R. G. Gann, W. M. Pitts (Eds.), *Evaluation of Alternative In-Flight Fire Suppressants for Full-Scale Testing in Simulated Aircraft Engine Nacelles and Dry Bays.* NIST SP 861, National Institute of Standards and Technology, 1994, pp. 345-465.

7. G. T. Linteris, G. W. Gmurczyk, in: R. G. Gann (Ed.), *Fire Suppression System Performance of Alternative Agents in Aircraft Engine and Dry Bay Laboratory Simulations.* NIST SP 890: Vol. II, National Institute of Standards and Technology, 1995, pp. 201-318.

8. T. A. Moore, A. Martinez, R. E. Tapscott, *Proceedings of the Options Technical Working Conference (HOTWC).* 1997, pp. 388-395.

9. N. Saito, Y. Ogawa, Y. Saso, R. Sakai, *Improvement on Reproducibility of Flame Extinguishing Concentration Measured by Cup Burner Method*, Report of Fire Research Inst. of Japan, No. 81, 1996, pp. 22-29.

10. S. Preece, P. Mackay, A. Chattaway, *Proceedings of the Halon Options Technical Working Conference (HOTWC)*, 2003.

11. J. A. Senecal, *Fire Safety Journal* 40 (2005) 579-591.

12. V. R. Katta, F. Takahashi, G. T. Linteris, in *Fire Safety Science: Proceedings of the Seventh International Symposium*. International Association for Fire Safety Science, 2003, pp. 531-544.

13. F. Takahashi, G. T. Linteris, V. R. Katta, Fourth International Symposium on Scale Modeling (ISSM-IV), Cleveland, OH, September 2003.

14. V. R. Katta, F. Takahashi, G. T. Linteris, *Combust. Flame* 137 (2004) 506-522.

15. G. T. Linteris, V. R. Katta, F. Takahashi, *Combust. Flame* 138 (2004) 78-96.

16. V. R. Katta, F. Takahashi, G. T. Linteris, *Combust. Flame*, 144, 645-661 (2006).

17. F. Takahashi, G. T. Linteris, V. R. Katta, 44th Aerospace Sciences Meeting and Exhibit, Reno, NV, AIAA-2006-0745, January 2006.

18. F. Takahashi, G. T. Linteris, V. R. Katta, "Extinguishment Mechanisms of Coflow Diffusion Flames in a Cup-Burner Apparatus," *Proc. Combust. Inst* 31 (2006), in press.

19. G. T. Linteris, F. Takahashi, V. R. Katta, *Proceedings of the Halon Options Technical Working Conference (HOTWC),* 2006.

20. V. R. Katta, W. M. Roquemore, *Proceedings of the Central States Section Meeting*. The Combustion Institute, 2006.

21. W. M. Roquemore, V. R. Katta, *Journal of Visualization* 2, No. 3/4 (2000) 257-272.

22. W. Tsang, V. Babushok, "Detailed mechanism for PAH species" *manuscript in preparation*, National Institute of Standards and Technology, Gaithersburg, MD, 2004.

23. Anon., *Computational Submodels, International Workshop on Measurement and Computation of Turbulent Nonpremixed Flames*, http://www.ca.sandia.gov/TNF/radiation.html, 2003.

24. V. R. Katta, L. P. Goss, W. M. Roquemore, *AIAA J.* 32 (1994) 84.

25. V. R. Katta, L. P. Goss, W. M. Roquemore, *Int. J. Num. Methods Heat Fluid Flow*, Vol. 4, No. 5, 1994, p. 413.

26. F. Takahashi, V. R. Katta, *Proc. Combust. Inst.* 30 (2005) 375-382.

27. R. W. Bilger, *Proc. Combust. Inst.* 22 (1988) 475.

28. F. Takahashi, V. R. Katta, *Proc. Combust. Inst.* 28 (2000) 2071-2078.

29. B. J. McBride, S. Gordon, "Computer Program for Calculation of Complex Chemical Equilibrium Compositions and Applications—II. Users Manual and Program Description," NASA RP-1311, June 1996.

30. F. Takahashi, V. R. Katta, *Proc. Combust. Inst.* 30 (2005) 383-390.

31. F. Takahashi, G. T. Linteris, V. R. Katta, "Vortex-Coupled Oscillations of Edge Diffusion Flames in Coflowing Air with Dilution," *Proc. Combust. Inst* 31 (2006), in press.